Physics Letters B 782 (2018) 143–148

Contents lists available at ScienceDirect

Physics Letters B

www.elsevier.com/locate/physletb

Abrupt phase change of the core rotation in the ^{143}Sm nucleus

S. Rajbanshi [a,*], R. Raut [b], H. Pai [c,**], Sajad Ali [c], A. Goswami [c], G. Gangopadhyay [d], S. Bhattacharyya [e], G. Mukherjee [e], S. Muralithar [f], R.P. Singh [f], M. Kumar Raju [g,1], P. Singh [h,2], R.K. Bhowmik [f]

[a] Department of Physics, Dum Dum Motijheel College, Kolkata 700074, India
[b] UGC-DAE Consortium for Scientific Research, Kolkata centre, Kolkata 700098, India
[c] Saha Institute of Nuclear Physics, HBNI, 1/AF, Bidhannagar, Kolkata 700064, India
[d] University of Calcutta, Kolkata 700009, India
[e] Variable Energy Cyclotron Center, Kolkata 700064, India
[f] Inter University Accelerator Centre, Aruna Asaf Ali Marg, New Delhi 110067, India
[g] Nuclear Physics Department, Andhra University, Visakhapatnam 530003, India
[h] Indian Institute of Technology, Kharagpur 721302, India

ARTICLE INFO

Article history:
Received 23 October 2017
Received in revised form 10 March 2018
Accepted 4 May 2018
Available online 29 May 2018
Editor: D.F. Geesaman

Keywords:
Magnetic rotation
Lifetime measurement
Shears mechanism with the principal axis cranking model
^{143}Sm

ABSTRACT

Dipole sequences in the ^{143}Sm nucleus have been investigated via the ^{124}Sn (^{24}Mg, 5n) reaction at E_{lab} = 107 MeV using the Indian National Gamma Array (INGA). The spin-parity of the associated levels have been firmly established from the spectroscopic measurement. Level lifetimes of several levels in the dipole bands have been measured using the Doppler Shift Attenuation Method. The decreasing trend of the measured $B(M1)$ and $B(E2)$ transition strengths in one of the sequence (DB I) spells out its origin as Magnetic Rotation (MR). Though, the trends of $B(M1)$ and $B(E2)$ in DB I are reproduced well in the theoretical calculations using the Shears mechanism with the Principal Axis Cranking (SPAC) model, the calculations fail to reproduce the sharp rise in the $B(M1)/B(E2)$ ratio at the highest spins in DB I. Such rise in the $B(M1)/B(E2)$ values is in well agreement with the theoretical calculations within the shears mechanism as prescribed by the Clark and Macchiavelli considering the smooth decrease of the core rotation along the sequence. The experimental observations along with the theoretical calculations for the second dipole band (DB II), indicate that the core rotation, rather than the shears mechanism, is being favored for angular momentum generation. This represents a unique observation of forking of the shears band DB I from an abrupt phase change of the core from spherical into the deformed one.

The observation of band-like structure in weakly deformed nuclei near shell closures has long been of interest in nuclear structure studies. These nuclei, generally, do not have an asymmetry in mass distribution, like the mid-shell ones which break the rotational symmetry and consequently exhibit regular sequences characterized by $E2$ intraband transitions in their level structure [1–3]. In the spherical or weakly deformed nuclei in the vicinity of the shell closures, the current distribution of few nucleons (particles and/or holes) outside the core crucially contribute in the generation of angular momentum and several exotic phenomena have been observed in such systems [4].

The "shears mechanism", following a detailed experimental and theoretical investigations [5–7], has been identified as one of such phenomena associated with the generation of angular momentum in nuclei with few particles and holes outside a weakly deformed core. The manifestation of the mechanism has been established as a regular sequence of levels connected by strong $M1$ intraband transitions while the cross-over $E2$ transitions are either weak or absent in conformity with the weak deformation characteristics in these nuclei. As is now understood, particles and holes outside the

* Corresponding author at: Department of Physics, Dum Dum Motijheel College, Kolkata 700074, India.
** Corresponding author at: Saha Institute of Nuclear Physics, 1/AF Bidhannager, Kolkata 700 064, India.
E-mail addresses: subhphy@gmail.com (S. Rajbanshi), h.pai@saha.ac.in (H. Pai).
[1] Presently at Research Center for Nuclear Physics, Osaka University, Japan.
[2] Presently at IRFU, CEA, Université Paris-Saclay, F-91191 Gif-sur-Yvette, France.

https://doi.org/10.1016/j.physletb.2018.05.021

weakly deformed core can form an arrangement of two perpendicularly aligned angular momentum vectors (blades) that represent the band head configuration of the band. Angular momentum along the band is generated by closing-in of the two blades, much like that of a pair of shears that renders the name shears band to the resulting sequence. Such an arrangement of particle and hole angular momentum leads to a large transverse component of the magnetic dipole moment (see, for example, Fig. 4 of Ref. [4]) that explains the strong intraband $M1$ transitions observed in the bands. This transverse component of the magnetic dipole moment decreases in magnitude with the closing-in of the angular momentum vectors thus explaining the decreasing trend of the $B(M1)$ values along the band. The perpendicular component of magnetic dipole moment of the valence nucleons rotates about the total angular momentum axis and hence identified as Magnetic Rotational (MR) band. The MR bands terminate when the two blades are completely aligned to the total angular momentum vector generating the maximum possible spin corresponding to the particle-hole configuration assigned to the respective MR band [4]. The experimental signature of the MR band structure is a decreasing trend of the $B(M1)$ and $B(E2)$ values with increasing spin and the same has been well interpreted within the theoretical framework invoked for the purpose [4,8].

Though the nuclei in the vicinity of the shell closures do not have a stable deformation in the ground state, the excited multi-quasiparticle configurations involving high-j deformation driving orbitals, associated with MR bands, can extend a polarizing effect on the core leading to a weak deformation of the latter, manifested in the weak cross-over $E2$ transitions in these bands. In fact the total angular momentum of the constituent states in MR bands has contributions not only from the aligning angular momentum vectors generated by particles and holes but also from the rotation of the weakly deformed core. As the current distributions of the particles and the holes become more symmetric along the MR band, their polarizing effect correspondingly decreases and the same is indicated by the diminishing $B(E2)$ strengths with increasing spin in the MR bands. Interestingly, however, the $B(M1)/B(E2)$ ratio also exhibits a decreasing trend along the band thus implying an increasing core contribution along the MR sequence. This is appropriately interpreted by the Shears mechanism with Principal Axis Craking (SPAC) model that has been successfully applied to the MR bands observed in ^{139}Sm, ^{141}Eu and ^{142}Gd [9–11]. Quite uniquely, contrary to the aforementioned generality in the trend of the $B(M1)/B(E2)$ ratio along the MR bands, a smooth increase in this ratio has been observed in one of the dipole sequences in the ^{144}Dy nucleus [12]. This band was ascribed to the MR phenomenon but no conclusive explanation could be presented for the idiosyncrasy. In the wake of such observations, a probe into the role of core rotation in the MR phenomenon, its contribution in the generation of angular momentum therein and its evolution along the band is warranted.

The present paper reports such a study in the ^{143}Sm ($Z = 62$, $N = 81$) nucleus. The nucleus was previously studied by Raut et al. [13] using heavy-ion induced fusion-evaporation reaction and an array of six Compton suppressed Clover detectors as the detection system. A dipole band, with a band-head energy of $\sim$ 8.6 MeV and tentative spin-parity $43/2^-$ was reported therein. The band was tentatively interpreted in the light of the MR phenomenon but, in the absence of any lifetime measurements, no conclusive evidence for the proposition could be obtained. The current work re-investigates the dipole structure (DB I) in ^{143}Sm using an array of higher efficiency provides confirmation to the MR mechanism associated with the sequence and reports a new dipole band (DB II) feeding DB I, at one of its intermediate states. Such bifurcation in the level structure is understood to embody a novel behaviour of this nucleus in the generation of angular momentum at the highest excitations.

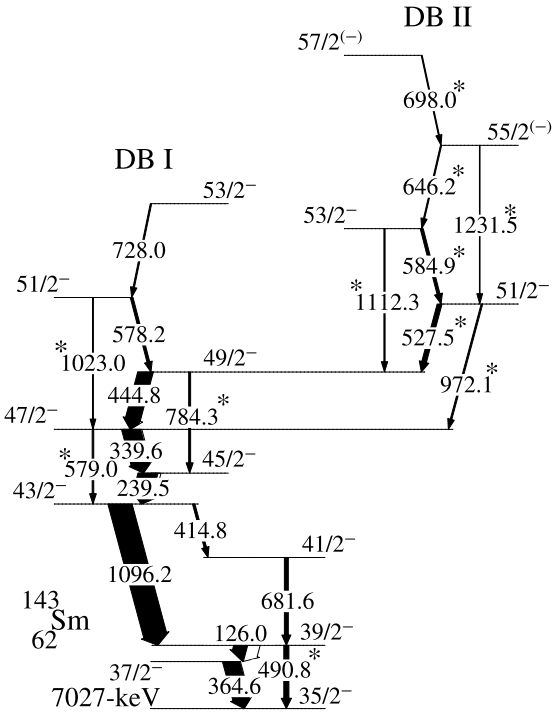

Fig. 1. The proposed level structure of the negative parity states above the 7027-keV $35/2^-$ state in ^{143}Sm. The newly observed transitions are marked by an asterisk.

The dipole structures in ^{143}Sm were populated in the present study using ^{124}Sn(^{24}Mg, 5n) reaction at $E_{lab} = 107$ MeV. The beam was obtained from the 15 UD pelletron at the Inter University Accelerator Center (IUAC), New Delhi. The target was 0.8 mg/cm^2 enriched (99.9%) ^{124}Sn evaporated on a 13 mg/cm^2 gold backing. The residues were produced with velocity $\beta \sim 1.6\%$. The de-exciting γ transitions were detected using the Indian National Gamma Array (INGA) which consisted of eighteen Compton suppressed clover detectors arranged in four different angles 90°(6), 123°(4), 148°(4) and 57°(4) with respect to the beam axis (the number in the parenthesis is the detector numbers at the respective angles) [14]. About 8×10^8 two and higher fold γ–γ coincidence events were collected in list mode format. The acquired data was sorted into different symmetric and angle dependent E_γ–E_γ matrices with INGASORT [15] software and subsequent analysis was performed using the INGASORT [15] and RADWARE [16,17] codes. The multipolarities and the electromagnetic characters of the observed γ-ray transitions, for assigning the spin-parity of the levels, were determined from the measurements of the ratio for Directional Correlation from Oriented (R_{DCO}) state [18,19], the asymmetry in linear polarization (Δ) [20–23] and the mixing ratio (δ) [24–26]. The experimental details and data analysis procedures have been described in details in Ref. [27,28].

The proposed dipole bands in ^{143}Sm, as observed in the present work, is illustrated in Fig. 1. In the previous study [13] the spin-parity assignments of the associated levels were tentative owing to the large uncertainties or impossibilities in the R_{DCO} and polarization asymmetry measurements of transitions, such as 126 keV, leading to the dipole band. In the current investigation, the 490.8 keV transition has been observed de-exciting the same 7517 keV level as the 126 keV transition. The R_{DCO} and polarization asymmetry values of this 490.8 keV γ-ray establish its $E2$ character, following which the spin-parity of the 7517 keV level could be confirmed to be $39/2^-$, upholding the previous (tentative) assign-

ment by Raut et al. Further, the R_{DCO} and polarization asymmetry values for the 1096.2, 414.8 and 681.6 keV transitions are consistent with the previous assignments and consequently the spin-parity of the 8614 keV state has been conclusively assigned as $43/2^-$.

Raut et al. had reported a dipole sequence in the ^{143}Sm nucleus starting at 8614 keV level and extending upto a spin of $57/2^-$. The R_{DCO}, polarization asymmetry and multipole mixing ratio of the first four member transitions of this band, 239.5, 339.6, 444.8 and 578.2 keV, determined in the present study establish their predominantly $M1$ nature in compliance with the earlier assignments and confirming the spin-parity of the sequence upto $51/2^-$. Above this state, Raut et al. had assigned three $M1$ transitions, 602, 728 and 706 keV, to the dipole band. The present work, carried out using a substantially more sensitive detection setup, has confirmed the 728.0 keV transition as a member of the dipole band above $51/2^-$ state while the 602.0 and 706.0 keV transitions are placed above the $51/2^-$ 10213.7-keV and $49/2^-$ 9635.5-keV excited states, in parallel with the 728.0 and 578.2-keV in-band transitions, respectively. Measured R_{DCO}, and Δ values for the 728.0-keV transition have been confirmed the spin-parity of $53/2^-$ for the highest observed state of the band designated as DB I. We have also observed the weak cross-over transitions between $47/2^- \rightarrow 43/2^-$, $49/2^- \rightarrow 45/2^-$ and $51/2^- \rightarrow 47/2^-$ states in DB I (Fig. 1). The R_{DCO} and polarization asymmetry measurements of these confirm their $E2$ character.

The salient finding of the present work is the observation of a bifurcation in DB I at $49/2^-$ leading to another sequence of levels connected by the 527.5, 584.9, 646.2 and 698.0 keV transitions. The R_{DCO} and polarization asymmetry measurements of 527.5 and 584.9 keV γ-rays indicate their predominantly $M1$ nature. The polarization asymmetry of 646.2 and 698.0 keV transitions could not be determined owing to the want of statistics at these highest excitations but the R_{DCO} values for these do indicate their dipole character. Following these assignments, the sequence of levels forked from DB I has been interpreted as the second dipole band, labelled as DB II in Fig. 1. Cross-over transitions connecting $53/2^- \rightarrow 49/2^-$ and $55/2^- \rightarrow 51/2^-$ states (Fig. 1) in DB II have also been observed with statistics that did not allow for determination of their polarization asymmetry but did qualify for the extraction of the R_{DCO} values that confirm their quadrupole character.

Observation of Doppler-broaden lineshape corresponding to the γ-rays in DB I and DB II facilitated the determination of level lifetimes in these bands using the Doppler Shift Attenuation Method (DSAM). A combination of developments reported in [29] and the LINESHAPE [30,31] package has been used for the corresponding analysis. The stopping of the residue through the target and the backing media were simulated using Monte Carlo based codes and updated stopping powers from the SRIM database. The simulated trajectories were then used to generate velocity profiles of the residual nuclei (^{143}Sm) for the clover detectors at different angles by assuming that the response of a composite clover detector was identical to a single-crystal high-purity germanium (HPGe) detector with the dimension same as the dimension of the former placed at the same distance. The validity of this assumption was checked by analyzing the Doppler shapes obtained from a single crystal of a particular clover detector in the array [27] and comparing the lifetime results with that obtained from using the clover.

The velocity profiles were used as input parameter to calculate the expected Doppler shapes for transitions of interest. The level lifetimes were finally determined by the least square fitting of the experimental (gated) spectra with the calculated shapes. It is understood that if the spectrum is from a gate on a transition below (GTB) the transition of interest, it is necessary to incorporate the contributions from the side feeding transitions while analyzing the level lifetime. For analysis with GTB, as far as the LINESHAPE package is concerned, the side feeding is modelled with a cascade of five transitions and the moment of inertia of the sequence is typically chosen to be similar to that of the band of interest being analyzed. The same procedure has been adopted in the present work for determining the level lifetimes in DB I and DB II. In this process, the effect of variation in the side-feeding intensity between two extreme values (taking the corresponding uncertainties in intensities into account) resulted in a change in the evaluated level lifetime by less than 10%. The detail analysis procedure was discussed in Refs. [27,28].

In the fitting process, the particular situation is occurred for the level which is populated by more than one γ transitions (for example, $51/2^-$ of DB II which decays via the 527.5-keV transition which is populated by the 584.9 and 1231.5-keV transitions de-exciting from the $53/2^-$ and $55/2^{(-)}$ levels of DB II, respectively) and both of them have level lifetime. In the fitting process, one transition has been considered as in-band transition whereas other transition is representative of the observed side-feeding transition. This information has been incorporated in the feeding history of the level of interest by replacing the lifetime of the top feeding in-band level with the intensity weighted average of the lifetimes of the states through which the transitions decay.

The side feeding lifetime is often identified as one of the principal uncertainties in the analysis of DSAM data. However, if the spectrum is generated from a gate on a transition that is atop (GTT) the transition of interest the effect of the side feeding is eliminated. Such spectra with gates on the higher lying transitions, above the transitions of interest, are plagued with lack of statistics, and it is often impossible to use these for lifetime analysis. In the present work, level lifetimes of some of the levels, both in DB I and DB II, could actually be extracted from both GTB and GTT spectra. These were $45/2^-$, $47/2^-$ and $49/2^-$ states in DB I and $51/2^-$, $53/2^-$ states in DB II. This analysis facilitated extraction of side feeding times required for determination of level lifetimes from GTB spectra. The lifetime of these levels were first determined using GTT spectra and then using the GTB ones, for different values of the side-feeding times, in order to reproduce the result obtained from the GTT. In the process, the side feeding time required for the GTB based analysis, was extracted. For the remaining states, where both the GTT and the GTB techniques could not be applied and the lifetime had to be determined only from the GTB, the value of the side feeding time used was determined from an extrapolation of the measured values of the same from the previous analysis [32].

Table 1 summarizes the R_{DCO}, Δ, and the lifetime results from the present measurements along with the $B(M1)$ and the $B(E2)$ values in bands DB I and DB II in ^{143}Sm. Fig. 2 illustrates typical fits to the experimental Doppler affected spectra that were simultaneously fitted at three different angles, 148^o, 123^o and 90^o, to obtain lifetime results. The uncertainties on the quoted lifetimes were derived from behaviour of the χ^2 value in the vicinity of the least square minimum. The uncertainties do not include the systematic contribution of the stopping powers that, owing to the use of updated and experimentally bench marked stopping powers from the SRIM database, are expected to be $\sim$ 5%. The absence or non-observation of the cross-over ($E2$) transition $53/2^- \rightarrow 49/2^-$ in DB I actually results in a large value of the $B(M1)/B(E2)$ ratio for the $53/2^-$ state. The lower limit of this value can be estimated from the minimum intensity of the transition required for observing it in the coincidence spectrum. In the present data, we were able to observe the γ-ray transitions with minimum intensity at 1% with respect to that of the 239.5 keV transition. Considering this to be the maximum intensity of the unobserved cross-over transition, the lower limit of the ratio of the $B(M1)$ and the $B(E2)$

Table 1
The DCO ratio (R_{DCO}), polarization asymmetry (Δ), level lifetimes (τ) and side feeding lifetimes (τ_{sf}) of the states and the corresponding $B(M1)$, $B(E2)$ and $B(M1)/B(E2)$ transitions rates for the γ transitions of the dipole bands DB I and DB II in ^{143}Sm.

J_i [$\hbar$]	J_f [$\hbar$]	E_γ [MeV]	R_{DCO} [a]	Δ	Branching [%]	τ [ps]	τ_{sf} [ps]	$B(M1)$ [μ_N^2]	$B(E2)$ [e^2b^2]	$B(M1)/B(E2)$ [μ_N^2/e^2b^2]
DB I										
$45/2^-$	$43/2^-$	239.5	$0.56(3)^Q$	−0.21(16)	100	$1.02^{+0.16}_{-0.12}$	0.20(3)[b]	$3.52^{+0.55}_{-0.42}$		
$47/2^-$	$45/2^-$	339.6	$0.52(3)^Q$	−0.27(4)	92.3	$0.58^{+0.09}_{-0.08}$	0.21(3)[b]	$2.16^{+0.34}_{-0.28}$		$12.70^{+2.50}_{-2.22}$
	$43/2^-$	579.0			7.7				$0.17^{+0.02}_{-0.02}$	
$49/2^-$	$47/2^-$	444.8	$0.48(4)^Q$	−0.12(4)	85.8	$0.44^{+0.07}_{-0.06}$	0.18(3)[b]	$1.20^{+0.20}_{-0.16}$		$13.33^{+3.70}_{-2.31}$
	$45/2^-$	784.3	$1.70(15)^D$	+0.32(11)	14.2				$0.09^{+0.02}_{-0.01}$	
$51/2^-$	$49/2^-$	578.2	$1.27(10)^D$	−0.08(3)	85.4	$0.41^{+0.07}_{-0.06}$	0.16(4)[c]	$0.61^{+0.10}_{-0.09}$		$20.33^{+4.91}_{-4.20}$
	$47/2^-$	1023.0		+0.11(3)	14.6				0.03(1)	
$53/2^-$	$51/2^-$	728.0	$1.09(9)^D$	−0.04(2)	100	0.78↓	0.13(3)[c]	0.18↑		46.78↑[d]
DB II										
$51/2^-$	$49/2^-$	527.5	$0.45(4)^Q$	−0.26(8)	74.8	$0.78^{+0.12}_{-0.09}$	0.15(3)[b]	$0.36^{+0.06}_{-0.04}$		$12.00^{+2.61}_{-1.96}$
	$47/2^-$	972.1	$1.81(23)^D$		25.2				0.03(1)	
$53/2^-$	$51/2^-$	584.9	$0.42(4)^Q$	−0.12(5)	73.6	$0.57^{+0.09}_{-0.07}$	0.16(4)[b]	$0.35^{+0.06}_{-0.04}$		$17.50^{+3.91}_{-3.04}$
	$49/2^-$	1112.3	$2.09(21)^D$		26.4				0.02(1)	
$55/2^{(-)}$	$53/2^-$	646.2	$0.91(8)^D$		64.3	$0.44^{+0.07}_{-0.06}$	0.11(3)[c]	$0.31^{+0.05}_{-0.04}$		$15.50^{+3.49}_{-2.99}$
	$51/2^-$	1231.5	$1.77(20)^D$		35.7				0.02(1)	
$57/2^{(-)}$	$55/2^{(-)}$	698.0	$1.28(11)^D$		100	0.66↓	0.08(3)[c]	0.25↑		

The uncertainties are rounded off to the nearest value up to two decimal places.
[a] The measured R_{DCO} [$I_\gamma(148°)/I_\gamma(90°)$] value of the γ-transitions form the gate on quadrupole (Q) and dipole (D) transitions.
[b] Determined from level lifetime analysis using both GTT and GTB spectra, as discussed in the text.
[c] Determined from an extrapolation of the side feeding times measured for some of the levels indicated with b, as discussed in the text.
[d] The lower limit of the $B(M1)/B(E2)$ value has been extracted for the $53/2^-$ state of DB I from the intensity measurements.

values comes out to be of 46.78 $\mu_N^2/(eb)^2$, that has been recorded in Table 1.

The dipole band DB I in ^{143}Sm is characteristically similar to the MR bands observed in the neighbouring nuclei such as ^{139,141,142}Sm, ^{141,143}Eu, and ^{142}Gd [9–11,27,28,33]. The transitional probabilities, $B(M1)$ and $B(E2)$, in DB I exhibit the characteristic decrease with increasing spin, as illustrated in Fig. 3, identical to that for the MR bands in the aforementioned nuclei in the vicinity. In fact the values of $B(M1)$ and $B(E2)$ in DB I are comparable to those in the other MR bands identified in this mass region. These observations uphold the proposition that the DB I sequence in the ^{143}Sm nucleus is a MR band.

The dipole bands in this mass region have often been interpreted as MR bands on the basis of theoretical calculations within the framework of the Shears mechanism with Principal Axis Cranking (SPAC) model [10,11,27,28,33]. The same semiclassical calculation has been carried out for the dipole band DB I in ^{143}Sm, having assigned it a $\pi h_{11/2}^4 \otimes \nu h_{11/2}^{-1}\ \pi(g_{7/2}/d_{5/2})^{-2}$ configuration. The Total Routhian surface (TRS) calculation [34,35] exhibit a prolate minimum [$\beta_2 \approx 0.10$ at rotational frequency (ω) ≈ 0.200 MeV] associated with this configuration in ^{143}Sm nucleus. The excitation of four proton particles into the $h_{11/2}$ orbital is favored by the sharp decreasing trend of its energy at the aforementioned deformation and similar excitation's have previously been reported for ^{149}Gd ($Z = 64$, $N = 85$) nucleus [37] with deformation of the same order. The preferential alignment of the angular momentum vectors produced by the particle and the hole, under prolate deformation, is along the rotation axis and the deformation axis, respectively. The SPAC model, that has been elaborated elsewhere (Ref. [27,28], for example), pertains to the minimization of the total energy of an excited state with a given spin with respect to the angles of the two (particle and hole) angular momentum blades with rotation axis. The angles corresponding to the minimized energy are applied to determine the $B(M1)$ and $B(E2)$ values of the respective states. In the present case, the SPAC calculations have been performed with an unstretched condition of the hole and the particle angular momenta, $j_1 = 9.5\hbar$ and $j_2 = 14\hbar$, respectively. The resulting $B(M1)$, $B(E2)$ and rotational frequency (ω) for the band DB I well reproduce the experimental numbers, as illustrated in Fig. 3. The parameter values for this calculation have been adopted with reference to the similar efforts in the neighbouring nuclei [9–11, 27,28,33]. The successful representation of the decreasing trend of experimental $B(M1)$ and $B(E2)$ values with spin as well as the behaviour of ω therein, within the purview of the SPAC model, is strongly indicative of the fact that the maximum contribution to the angular momentum of the states constituting DB I is from

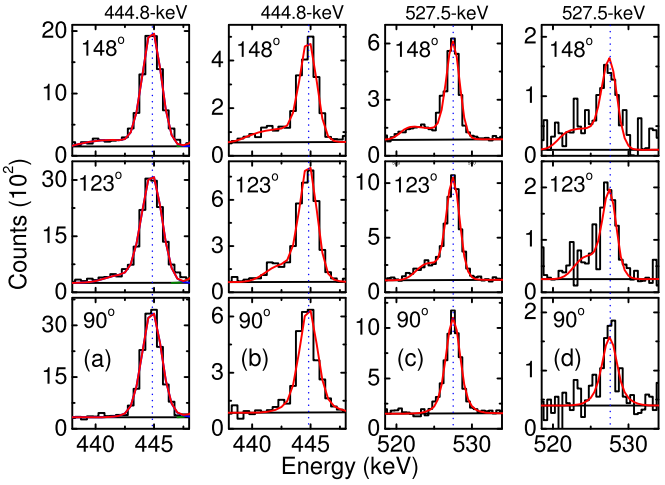

Fig. 2. (Color online.) The experimental spectra along with the fitted line shapes for the γ transitions (a) 444.8 and (c) 527.5-keV created by the "GTB" technique and, (b) 444.8 and (d) 527.5-keV created by the "GTT" technique of the bands DB I and DB II in ^{143}Sm. The top, middle and bottom rows correspond to the shapes in the 148°, 123° and 90° detectors, respectively. The obtained total line-shapes of the γ transitions are represented by the red lines.

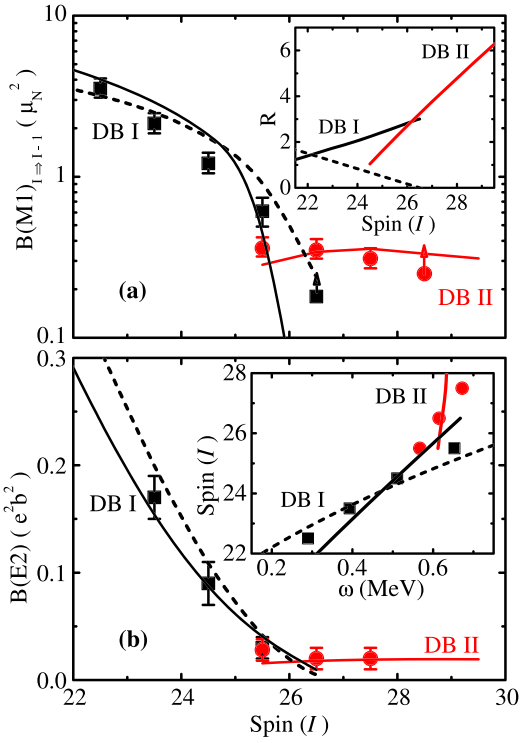

Fig. 3. (Color online.) Comparison of the experimental results for the dipole bands DB I (represented by the black filled squares) and DB II (represented by the red filled solid circles) in ^{143}Sm with the SPAC model (solid black and red lines for the DB I and DB II, respectively) and the Clark and Macchiavelli's description (black dashed lines). The $B(M1)$ and $B(E2)$ transition strengths against spin (I) have been depicted in (a) and (b), respectively. The variation of R with spin (I) and the dependence of spin (I) on the rotational frequency (ω) are shown in the inset of (a) and (b), respectively.

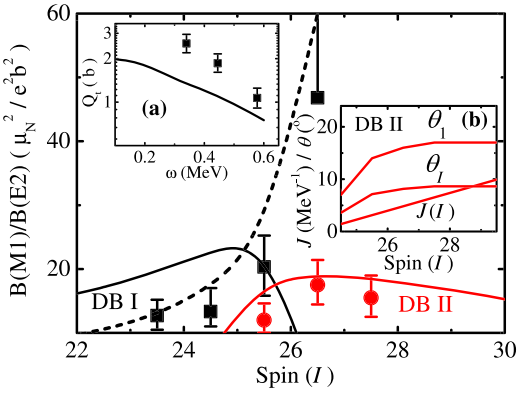

Fig. 4. (Color online.) Comparison of the experimental $B(M1)/B(E2)$ values for the dipole bands DB I (represented by the black filled squares) and DB II (represented by the red filled solid circles) in ^{143}Sm with the SPAC model (solid black and red lines for the DB I and DB II, respectively) and the Clark and Macchiavelli's description (black dashed lines). Inset (a) shows the experimental transition quadrupole moment parameter Q_t (solid black square) along with the results obtained from the TRS calculations (solid black line) for DB I. Inset (b) shows the moment of inertia of the core and the shears angles (θ_1 and θ_I) for the dipole band DB II.

the shears mechanism, thus confirming the earlier interpretation by Raut et al. [13]. However, it is intriguing to address the rapidly falling trend of the $B(M1)/B(E2)$ ratio at the highest spins in DB I, so predicted by the SPAC model calculation, and that is in sharp contradiction to the observed sharp rise of the same (Fig. 4). This decreasing trend of the $B(M1)/B(E2)$ value is due to the evolving contribution of the collective core rotation along the band as depicted in the inset of Fig. 3 (a). There is a precedence of reproducing the experimentally observed falling trend of $B(M1)/B(E2)$ in case of shears band in ^{139}Sm [9] by incorporating an increase in the collective contribution along the sequence. Therefore, the (reverse trend of) increase in the ratio, identified in the present investigation, might actually be indicative of a reduction in the core contribution along the DBI band in ^{143}Sm.

A confirmation to the proposition (on the evolving core contribution) was obtained from a further (semiclassical) calculation, following the prescription of the Clark and Macchiavelli [8], that was carried out for the DBI band in ^{143}Sm, ascribed to the $\pi h_{11/2}^4 \otimes \nu h_{11/2}^{-1}\ \pi(g_{7/2}/d_{5/2})^{-2}$ configuration. This calculation, at variance with the SPAC model, incorporates a smooth decrease in the core angular momentum (R) along the band as per the expression, $R = 2 \times (26.5 - I)/\xi$, ξ being the number of observed states in the band. The scalar addition of the (R) with the shears angular momentum ($|\vec{j_{sh}}| = |\vec{j_p} + \vec{j_h}|$; where $\vec{j_p}$ and $\vec{j_h}$ are the angular momentum vectors for the particles and the holes, respectively) produces the total angular momentum of the state (I). The transition probabilities are calculated from the equations elaborated in Ref. [8]. The results in the present case, carried out using $j_p = 16\hbar$, $j_h = 10.5\hbar$ and $\xi = 6$, are in excellent overlap with the experimental ω, $B(M1)$, $B(E2)$ and $B(M1)/B(E2)$ values in DBI, as illustrated in Figs. 3 and 4. It emerges that the angular momentum contribution from the collective rotation, R, is $\sim$2 at the bandhead $43/2^-$ and smoothly decreases to 0 at the highest observed state $53/2^{(-)}$. Similar decreasing feature of the transition quadrupole moment parameter Q_t has been obtained from the TRS calculation in agreement with the values derived from the present experimental results, as shown in the inset (a) of Fig. 4. This implies that the core becomes more and more symmetric, with respect to the total angular momentum, as the angular momentum blades close-in to generate the high spin states in DBI and thus leads to a reduction in the collectivity along the band DB I. Together, the SPAC and the Clark–Macchiavelli calculations affirm the MR character of the DBI band in ^{143}Sm along with a novel evidence of decreasing core contribution with increasing spin along the sequence.

However, if the $53/2^-$ state is not the member of the dipole band DB I the SPAC model calculation is in better agreement with the measured $B(M1)$ values throughout the band. This implies that the shears mechanism with the principal axis cranking may represents an alternative interpretation of generation of the angular momentum in the dipole band DB I and this alternative scenario cannot be ruled out.

The unique observation of the present study pertains to the dipole band DB II that bifurcates from DB I at $49/2^-$ and emerges as an energetically favoured sequence thereafter. The I vs. ω plot (Fig. 3) for this band illustrates generation of much angular momentum (I) with very little increment in the rotational frequency (ω), thus indicating an increase in the collectivity along DB II. Indeed, the SPAC calculations carried out for DB II, assigned with the same quasiparticle configuration as DB I, yield a satisfactory overlap with the experimental ω, $B(M1)$, $B(E2)$ and $B(M1)/B(E2)$ values (Figs. 3 and 4) only when the moment of inertia (J) of the core is allowed to increase with spin, as depicted in Fig. 4. This calculation conclusively establish that the increasing angular momentum along DB II entirely results from the increasing contribution of the core rotation therein as is indicated by the unit slope of R vs I plot in Fig. 3 while the orientation of the angular momentum blades (shears) is almost fixed throughout the sequence (Fig. 4). It may thus be stated that the DB II sequence represents a scenario where the collective core rotation is a more favored mechanism for generation of angular momentum rather than the alignment of the angular momentum blades underlying the MR/shears phenomenon. It is imperative to distinguish this

situation from those previously reported in ^{139,141}Sm [9,33] and ^{128}Ba [36] wherein an increase in collectivity have been observed along the MR bands in sharp contrast to the present case with one of the bands (DB I) preserving its MR origin to higher spins while evolving into as well as coexisting with an alternative and energetically favourable band (DB II) of collective rotational character.

The $49/2^-$ state in the ^{143}Sm nucleus, thus, represents a very unique transition point beyond which two radically different mechanisms for generation of angular momentum in nuclei appear to coexist. While the states of DB I beyond $49/2^-$ still originate from the aligning particle and hole angular momentum blades, as is the case in MR bands, the levels of increasing spin in DB II emerge from the collective rotation of the core. The latter being energetically favorable, the level at $49/2^-$ can be perceived as a transition point from a few quasiparticle based angular momentum generation, as in the shears mechanism, to a domain where the collective rotation of the core is the preferred mode of excitation. Equivalently, this also implies a transformation from a near spherical or weakly deformed system to a well deformed one. To the best of our knowledge, this is the maiden instance when such a transformation has been established in the study of high-spin excited states of atomic nuclei.

In summary, high spin dipole sequences in the ^{143}Sm nucleus have been investigated using heavy-ion induced fusion-evaporation reaction and an array of Compton suppressed Clover detectors. Two bands, DB I and DB II, have been confirmed from the spectroscopic measurements including determination of level lifetimes using DSAM. Theoretical calculations have been carried out within the purview of the SPAC model as well as the semiclassical model of Clark and Macchiavelli. In the light of the experimental observations and their successful representation in the model calculations, DB I has been confirmed as a MR band while DB II, stemming out of DB I at one of its intermediate state, has been ascribed to the collective rotation of the core and energetically more favored compared to the corresponding same spin states of DB I. The intermediate state of DB I, with spin $49/2^-$, has thus been identified as a transition point from a weakly deformed system, with shears mechanism in operation for generation of angular momentum, to a deformed one, with collective rotation as the preferred mode for producing higher spins albeit coexisting with the MR phenomenon in the same excitation regime. This is a unique observation of such transition followed by coexistence in the structure studies of atomic nuclei.

Acknowledgements

We would like to acknowledge the help from all INGA collaborators. We are thankful to the Pelletron staff for giving us steady and uninterrupted ^{24}Mg beam. S. R. would like to acknowledge the financial assistance from the University Grants Commission - Minor Research Project (No. PSW-249/15-16 (ERO)). G. G acknowledges the support provided by the University Grants Commission - departmental research support (UGC-DRS) program. H. P. is grateful for the support of the Ramanujan Fellowship research grant under SERB-DST (SB/S2/RJN-031/2016).

References

[1] A. Bohr, B.R. Mottelson, Phys. Rev. 90 (1953) 717.
[2] S. Raman, C.W. Nestor Jr, P. Tikkanen, At. Data Nucl. Data Tables 78 (2001) 1.
[3] N.J. Stone, At. Data Nucl. Data Tables 90 (2005) 75.
[4] S. Frauendorf, Rev. Mod. Phys. 73 (2001) 463.
[5] A.J. Simons, et al., Phys. Rev. Lett. 91 (2003) 162501.
[6] H. Hübel, Prog. Part. Nucl. Phys. 54 (2005) 1.
[7] A.K. Jain Amita, B. Singh, At. Data Nucl. Data Tables 74 (2000) 283.
[8] R.M. Clark, A.O. Macchiavelli, Annu. Rev. Nucl. Part. Sci. 50 (2000) 1.
[9] A.A. Pasternak, et al., Eur. Phys. J. A 37 (2008) 279–286.
[10] E.O. Podsvirova, et al., Eur. Phys. J. A 21 (2004) 1–6.
[11] A.A. Pasternak, et al., Eur. Phys. J. A 23 (2005) 191–196.
[12] M.G. Procter, et al., Phys. Rev. C 81 (2010) 054320.
[13] R. Raut, et al., Phys. Rev. C 73 (2006) 044305.
[14] S. Muralithar, et al., Nucl. Instrum. Methods Phys. Res., Sect. A 622 (2010) 281.
[15] R.K. Bhowmik, Ingasort Manual, private communication.
[16] D.C. Radford, Nucl. Instrum. Methods Phys. Res., Sect. A 361 (1995) 297.
[17] D.C. Radford, Nucl. Instrum. Methods Phys. Res., Sect. A 361 (1995) 306.
[18] A. Krämer-Flecken, et al., Nucl. Instrum. Methods Phys. Res., Sect. A 275 (1989) 333–339.
[19] M.K. Kabadiyski, K.P. Lieb, D. Rudolph, Nucl. Phys. A 563 (1993) 301–325.
[20] K. Starosta, et al., Nucl. Instrum. Methods Phys. Res., Sect. A 423 (1999) 16–26.
[21] Ch. Droste, et al., Nucl. Instrum. Methods Phys. Res., Sect. A 378 (1996) 518–525.
[22] J.K. Deng, et al., Nucl. Instrum. Methods Phys. Res., Sect. A 317 (1992) 242.
[23] P.M. Jones, et al., Nucl. Instrum. Methods Phys. Res., Sect. A 362 (1995) 556.
[24] T. Yamazaki, Nucl. Data. Sect. A 3 (1967) 1.
[25] E.D. Mateosion, A.W. Sunyar, At. Data Nucl. Data Tables 13 (1974) 392.
[26] E.S. Macias, W.D. Ruhter, D.C. Camp, R.G. Lanier, Comput. Phys. Commun. 11 (1976) 75–93.
[27] S. Rajbanshi, et al., Phys. Rev. C 90 (2014) 024318.
[28] S. Rajbanshi, et al., Phys. Rev. C 89 (2014) 014315.
[29] S. Das, et al., Nucl. Instrum. Methods Phys. Res., Sect. A 841 (2017) 17.
[30] J.C. Wells, N.R. Johnson, LINESHAPE: A Computer Program for Doppler Broadened Lineshape Analysis, Report No. ORNL-6689, 1991, p. 44.
[31] N.R. Johnson, et al., Phys. Rev. C 55 (1997) 652.
[32] R. Schwengner, et al., Phys. Rev. C 80 (2009) 044305.
[33] S. Rajbanshi, et al., Phys. Rev. C 94 (2016) 044318.
[34] W. Nazarewicz, J. Dudek, R. Bengtsson, T. Bengtsson, I. Ragnarsson, Nucl. Phys. A 435 (1985) 397.
[35] W. Nazarewicz, M.A. Riley, J.D. Garrett, Nucl. Phys. A 512 (1990) 61.
[36] O. Vogel, et al., Phys. Rev. C 56 (1997) 1338.
[37] S. Flibotte, et al., Nucl. Phys. A 530 (1991) 187.